Search for Slow Magnetic Monopoles with the NOνA Far Detector

A THESIS
SUBMITTED TO THE FACULTY OF THE GRADUATE SCHOOL
OF THE UNIVERSITY OF MINNESOTA
BY

Mohamed Elashri

IN PARTIAL FULFILLMENT OF THE REQUIREMENTS
FOR THE DEGREE OF
MASTER OF SCIENCE

Advisor: Dr.Alec Habig

August, 2020

Dedication

"Travel through the earth and see how Allah did originate creation"
Quran - [29:20]

To **Allah**, who created me for the purpose of exploring his world and for providing me with talents to do so.

To the **person** who existence in my world was the essential part of me. To who teach me all what I know about myself. to whom taught me about the world. Who will share first career step together forever.

To my **family**, who trust and support me along all my way.

To this **country** which gives me this opportunity.

Acknowledgements

Thanks to Allah, I had many people whom without, I wouldn't be able to do all this.

I owe my gratitude to my supervisor Dr.Alec Habig, who opened the door for me, who gave me the opportunity to work on magnetic monopole that was my passion since my high school. His guidance and valuable lessons about physics and life showed me what to be a great scientist.

I would like to thank my undergraduate professors, Dr. Ahmed Maarouf for his continuous inspiration. Dr. Ali Nassar who teach me most of the physics I know.

I want to express my deep gratitude towards Dr.Eric west for his support during my first graduate years and the deep discussions about physics which turned to hours of insight and, later, weeks of inspiration.

The work done here wouldn't be without the help I received from Dr. Martin frank, Dr. Gavin Davies and Justin Vasel. they taught me and went with me step by step and answered all my questions about NOνA.

I won't here without the support and help from my loving family. whose continuous support and prayers kept me working. I thank my father for always believing in me which is the fuel for me.

Abstract

The magnetic monopole is a hypothetical particle with a magnetic charge. It is an important field configuration in many Grand Unified Theories. Dirac in 1931 derived a charge quantization condition, which suggests that the existence of one magnetic monopole in the universe will explain electric charge quantization. Since then, a search of the elusive particle has begun, and yet all came with negative results. The NOνA Far Detector is able to probe some of the parameter space for the search for monopoles. To achieve this, two dedicated triggers, one for fast monopoles and the other for slow monopoles, have been developed to record signals. Results for the first 8 months of high-gain slow monopole data were obtained, and a 90% CL limit was established with no monopole observed. The analysis in this thesis is focused on new data with a higher gain, and we have explored potential improvement in efficiency and improvements in the reconstruction algorithm. We have done this analysis on Monte-Carlo generated simulated data to establish efficiencies and examined a control set of the new data to understand its differences from the old.

Contents

List of Tables

List of Figures

Chapter 1

Introduction and Physics of Magnetic Monopoles

This Thesis is divided into four main chapters; chapter one briefly presents the history of and science behind the magnetic monopoles. Chapter two, the NOvA experiment, is gives an explanation of the experiment's purpose, goal and the detector design. Chapter three gives an overview of the trigger system in NOνA and describes the slow Magnetic Monopole trigger within the experiment. The design and parameters are discussed with the current status of data collection methods. Chapter four hashes out the strategy for analysis and presents the data and simulated sets that will be used in the analysis. The main analysis and final results for this Thesis are presented. It discusses the improvement in the Monopole search within the new adjustment with comparison to the old results.

Magnetic Monopoles are particles with hypothetical magnetic charge. It is experimentally known that if we divide any magnet into a half up to subatomic level, it will always end up with north and south poles. Magnetic Monopoles are isolated magnets with only one pole, either south or north.

1.1 Introduction

The history of magnetism starts with the ancient world as there are many references to such phenomena in old civilizations, such as ancient Greece [1]. In 1819, the connection between electricity and magnetism was established by Oersted [2]. He discovered by accident that he could produce a magnetic field while the field was twitching a compass needle near a carrying electric current, it was called later the Oersted Experiment. Later this was formulated by Ampere in the famous Ampere's law equation, which also discovered that a magnetic field circulating in a closed path would produce a current flowing through a surface enclosed by that path [3].

The establishment of the four equations that fully describe classical electrodynamics theory came later by James Clerk Maxwell in his "A Treatise on Electricity and Magnetism" work in 1873 [4]. Initially, Maxwell assumed the existence of magnetic like charges to formulate his theory. However, magnetic charges have never been found in nature. When Maxwell unified classical electrodynamics in his four equations, he assumed that there are magnetic source charges like the electric charges. In 1931, Paul Dirac addressed the magnetic monopole in his famous paper [5]. Since then, many physicists have worked on the search for this elusive particle. All searches have so far failed to find the magnetic monopole. The last section of this chapter summarizes some of these trials.

1.2 Dirac Monopole

For many decades, physicists believed in the existence of magnetic monopoles, as it makes Maxwell's equation symmetric under the exchange of fields and their sources. In 1931, Dirac published a paper establishing a relationship between magnetic monopoles and the quantization of electric charges through quantum mechanics. In this first part of the paper, Dirac discussed one of the fundamental quantum mechanical properties, which is that the change in phase of a wave function around any closed curve must be the same for all wave functions, and it must be an arbitrary integral multiple of 2π [6].

Dirac's work results in a relation between the basic elementary electric charge e and the basic magnetic charge g as follows:

$$ge = \frac{n\hbar c}{2} \tag{1.1}$$

where n is an integer, then the quantity $g_D = \frac{\hbar c}{2e}$ is called the Dirac unit charge

After Dirac's Monopole paper, there were many other papers with different methods derived from the same Dirac quantization relation Eq. 1.1. Through this section, some of these methods are discussed, and first, the original Dirac derivation is presented then the quantization of angular momentum is used to derive the same result.

1.2.1 Dirac Derivation

Dirac introduced a derivation based on the magnetic vector potential argument and introduced a new concept called a Dirac string to deal with the singularities that arise. Dirac used two singular vector potentials for the magnetic monopole at the origin of the coordinate system:

$$A_{\pm} = g\frac{\pm 1 - cos\theta}{rsin\theta}\hat{\phi} \tag{1.2}$$

Dirac divided the space outside the monopole into two overlapping regions and wrote the last equation for the vector potential in each. These vector potentials are gauge-related. The northern region A_+ spans latitudes $0 \leq \theta \leq \pi - \epsilon$ and the southern region spans $\epsilon \leq \theta \leq \pi$ The two potentials are gauge-equivalent:

$$A_+ - A_- = \frac{2g}{rsin\theta}\hat{\phi} = 2g\nabla\phi \tag{1.3}$$

As the two potentials are gauge-equivalent they lead to the same magnetic field B

$$
\begin{aligned}
B = \nabla \times A_{+or-} &= \nabla \times (g(\pm 1 - cos\theta)\nabla\phi) \\
&= g(\nabla(\pm 1 - cos\theta)) \times \nabla\phi \\
&= g\frac{sin\theta}{r}\hat{\phi} \times \frac{1}{rsin\theta}\hat{\phi} \\
&= g\frac{1}{r^2}\hat{r}
\end{aligned} \tag{1.4}
$$

It is known that in quantum mechanics that a gauge transformation of a vector potential must be combined with a phase transformation of the wave function of the charged particle. Hence, using the two gauge-related vector potentials in Eq. 1.2 forces the use of two wave functions ψ_+ for $0 \leq \theta \leq \pi - \epsilon$ and ψ_- for $\epsilon \leq \theta \leq \pi$. In the overlap region $\epsilon \leq \theta \leq \pi - \epsilon$ the two wave function related by a gauge transformation

$$\psi_+ = \psi_- e^{\frac{2ige\phi}{\hbar c}} \tag{1.5}$$

In order for this equation to make sense physically, a wave functions $\psi_\pm$ must be single-valued and continuous. Based on that this happens only if $(4\pi ieg/\hbar c)$=1. This results in the electric charge quantization condition as $e^{(4\pi ieg/\hbar c)} = e^{2\pi in} = 1$ and this gives Eq 1.1.

1.2.2 Dirac's original derivation

The Dirac quantization condition can be derived by quantizing the angular momentum carried by electromagnetic fields [7] [8]. If an electric charge e at the origin and a magnetic charge g are separated by distance d this will result in electric and magnetic fields as follows :

$$
\begin{aligned}
E &= \frac{1}{4\pi\epsilon_0}\frac{e}{r^2}\hat{r} \\
B &= \frac{1}{4\pi}\frac{g}{r_b^2}\hat{r_b}
\end{aligned} \tag{1.6}
$$

Now place a magnetic charge g on the z-axis a distance d from the electric charge e, then its location is $d\hat{z}$, $r_b = r - d\hat{z}$. Then :

$$
\begin{aligned}
r_b &= \sqrt{(x+d)^2 + y^2 + z^2} \\
&= \sqrt{r^2 - 2xd + d^2} \\
&= r\sqrt{1 - \frac{2xd}{r^2} + \frac{d^2}{r^2}} \\
&\approx r(1 - \frac{xd}{r^2}) \\
&= r - \frac{xd}{r}
\end{aligned}
\tag{1.7}
$$

Then the total angular momentum of the system is:

$$
\begin{aligned}
L &= \frac{1}{c^2}\int r \times (E \times H) d^3x \\
&= \frac{1}{c^2}\int r \times (\frac{1}{4\pi\epsilon_0}\frac{e}{r^2} \times H) d^3x \\
&= \frac{e}{4\pi\epsilon_0}\int \frac{1}{r}(\hat{r}(\hat{r}.H) - H(\hat{r}.\hat{r})) d^3x \\
&= \frac{e}{4\pi}\int \frac{1}{r}(\hat{r}(\hat{r}.B) - B) d^3x
\end{aligned}
\tag{1.8}
$$

After some manipulation Eq. 1.8 gives

$$
\begin{aligned}
L &= \frac{e}{4\pi}\int \hat{r}(\nabla.B) d^3x \\
&= \frac{eg}{4\pi}\int \hat{r}\delta^3(r - d\hat{z}) d^3x \\
&= \frac{eg}{4\pi}\hat{z}
\end{aligned}
\tag{1.9}
$$

Now, if the angular momentum is quantized in the units of $\hbar$, it gives the Dirac quantization condition in Eq. 1.1.

1.2.3 Magnetic Coupling

For Dirac quantization condition 1.1, the minimal magnetic charge is for $n = 1$ which can be defined as

$$g_D = \frac{\hbar c}{2e} = \frac{e}{2\alpha_e} = 68.5e \tag{1.10}$$

where α_e is the fine structure constant $\alpha_e = e^2/\hbar c = 1/137$ and e is the minimal electric charge. If there existed a free quark with $e/3$, then it would be expected that the minimal magnetic charge would be three times larger. This minimal magnetic charge is very large compared with a minimal electric charge, and although magnetic monopole if exists makes a symmetric Maxwell's equations, it leads to numerical asymmetry in the context of the magnetic and electric effects. The magnetic fine structure constant is $\alpha_m = g^2/\hbar c = 34.25$. This is a very large coupling constant compared to electromagnetic interactions for electric charges, Magnetic and electromagnetic interactions thus are very strong and do not allow the use of perturbative techniques. As an example, the problem of elastic scattering of an electron by a magnetic monopole cannot be described by the exchange of one photon, but can be described if considering the exchange of many photons. This is due to the fact that $\alpha_m \alpha = \mathcal{O}(1)$, while in ordinary electron-electron scattering it has $\alpha^2 \approx \mathcal{O}(10^{-4})$. This means that the coupling of a magnetic monopole is about 4,690 times stronger than the coupling of an electric charge. This can explain why it is very hard to separate dipole magnet into individual poles (monopoles) and could explain why no magnetic monopoles have yet been discovered.

1.3 Grand Unified Theory and Monopoles

There are four fundamental forces in nature, weak and strong nuclear forces, the electromagnetic force, and gravity. Physicists are trying to formulate a theory that could explain all the forces. Many developments in this direction to find what is called a Grand Unified Theory (GUT) lead to establishment between GUTs and the existence of magnetic monopoles. 't Hooft [9] and Polyakov [10] demonstrate the existence of the magnetic monopole as a result of most GUTs and predict many properties of these magnetic monopoles which were not determined in Dirac's theory. In this section, an overview of the properties of GUT magnetic monopoles are given.

1.3.1 GUT Magnetic Monopoles

Magnetic monopoles have been discovered as solutions of gauge symmetry breaking in many Non-Abelian gauge theories, which includes GUTs theories by 't Hooft and Polyakov independently. It is known that GUT theories have a large group of exact gauge symmetries that mix the electroweak and strong interactions. All these symmetries are spontaneously broken at short distances or order M_x^{-1}, or at a large Mass of M. This can be seen as that each Non-Abelian group is broken to give U(1) theory at low energy with the field equations provides magnetic monopole solution. Magnetic monopole properties depend on the distance scale of the spontaneous symmetry breaking.

Dirac Monopole mass is a free parameter, but GUT monopole mass is not. It is possible to calculate monopole mass given a GUT model. The distance scale is estimated to be about 10^{14} GeV, for this magnetic monopole mass will be about 10^{16} GeV. This monopole is a very massive particle and is impossible to produce in particle accelerators given our current energy scale. GUT monopole properties can be summarized as follows, given that M_x is the grand unification energy scale, and α_x is the coupling constant at this energy. The parameters of GUT monopole are summarized in Tab. 1.1.

Charge	Mass	Size
g $= g_D$	$M \approx \frac{M_x}{\alpha_x} \approx 10^{16}$	$R \approx M_x^{-1} \approx 10^{-30}$ m

Table 1.1: GUT monopole properties

Some GUT models predict the possibility of magnetic monopoles to catalyze proton decay process. A typical monopole-catalyzed proton decay reaction is:

$$g_m + p \rightarrow g_m + e^+ + \pi^0 \tag{1.11}$$

In the Standard Model (SM), protons are stable because of the conservation of baryon number. But GUT magnetic monopoles contain Grand unified gauge plus Higgs fields, and most GUT models predict violation of baryon number conservation. It is believed that GUT monopoles would catalyze proton decay processes by increasing the rate of decay [11].

1.3.2 GUT Monopoles and Cosmology

As mentioned in the last section, the monopole mass is enormous, which means that it is impossible to be produced using current experimental methods. The only possibility to produce GUT monopoles is during early times $t \approx 10 \times 10^{-34}\,\mathrm{s}$ of the big bang epoch. At this early time, the universe was extremely hot and the energy density was high enough to produce such heavy particles. Looking for a signature for GUT monopoles from this epoch is very difficult due to the fact that inflation would dilute the density of GUT monopoles produced in the early universe [12].

1.4 Magnetic Monopole Search Techniques

In Tab. 1.1, the properties of magnetic monopoles are given. There are no constraints on velocity. It could be any velocity below the speed of light and is heavily dependent on mass. There are several techniques developed for monopole searches. There are three major categories: Proton decay, Induction, and Ionization. They correspond to model dependency. An induction experiment searches for any particles possessing a magnetic charge, thus they are not model dependent. Ionization experiments assume that monopole energy loss is larger than the minimum ionizing energy loss due to the large magnetic charge imposed by the Dirac quantization condition. As explained before, proton decay based experiments will be heavily dependent on model with the main assumption that the proton decays; these experiments are observing the number of proton decays, which will produce π_0's as in Eq. 1.11. These pions will be produced along the trajectory of the monopole. From there, the velocity of the monopole can be reconstructed by measuring the particle's time of flight inside the detector [14].

1.5 Present Limits on Magnetic Monopole Search

There have been no magnetic monopoles discovered and no confirmed evidence for magnetic monopoles. Only one experiment detected a monopole signal. Blas Cabrera took a superconducting loop at Stanford in 1982, placed it in an ultra-low magneticfield device, and monitored the current with a Superconducting Quantum Interference Device for many months. He observed a signal but it was not repeated or confirmed [13]. The lack of confirmed signals results in limits on the maximum possible monopole flux as a function of phase space parameters (mass and velocity).

The MACRO experiment [15] performed a search for heavy GUT monopoles. The flux limit results are summarized in Tab. 1.2. The experiment has a lot of sensitivity coverage for much of phase space, as shown in Fig. 1.1. Due to the fact that the MACRO detector was underground, it was not sensitive to low energy magnetic monopoles as they will be absorbed by the earth and then will not reach the detector.

Flux ($cm^2 s^{-1} sr^{-1}$)	m (GeV/c^2)	β
$\leq 1.4 * 10^{-16}$	$\gtrsim 10^{10}$	$> 10^{-10}$
$\leq 1.4 * 10^{-16}$	$\gtrsim 10^{16}$	$> 10^{-4}$
$\leq 2.8 * 10^{-16}$	$\gtrsim 10^{6}$	$> 10^{-1}$
$\leq 2.8 * 10^{-16}$	$\gtrsim 10^{10}$	$> 10^{-4}$

Table 1.2: MACRO Flux limit results, for each beta and mass parameter in the region where MACRO is sensitive, the limit of flux is calculated and reported in the flux column [15]

.

The IceCube experiment's [16] main search is for extra-galactic neutrinos. It is a large detector under the surface of the South Pole. Because of the huge detector surface area, it has 90% CL sensitivity for upper limit of 3×10^{-18} $cm^{-2}s^{-1}sr^{-1}$ for monopoles with $\beta \gtrsim 0.8$. Figure 1.1 also shows an approximation of the flux upper limit flux for monopoles with less than $\beta = 0.8$ with different experiments.

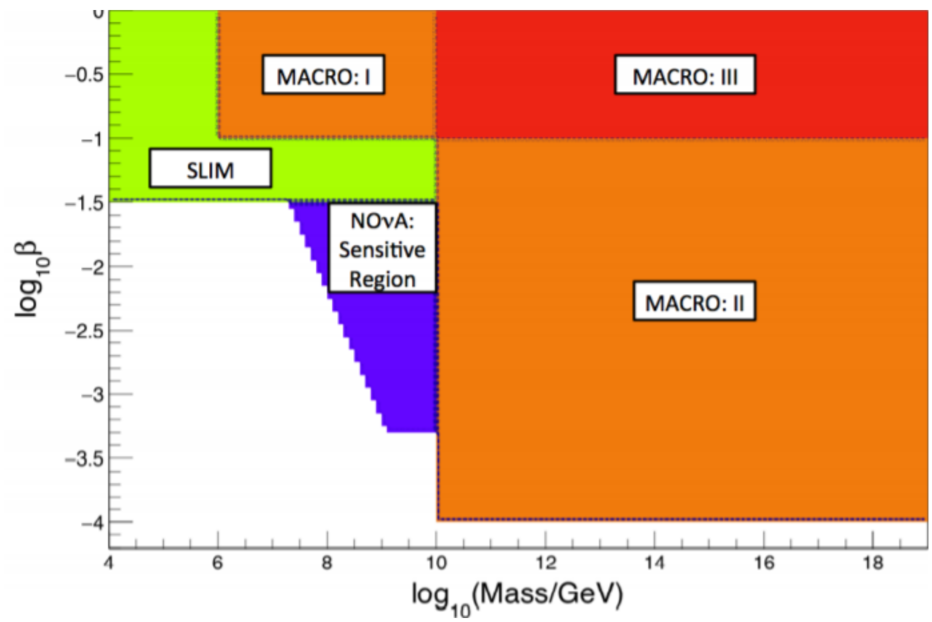

Figure 1.1: The upper flux limits at 90% CL of searches for non-relativistic ($\beta < 0.8$) monopoles as a function of monopole mass and velocity, set by MACRO and SLIM [14, 15, 16].

The SLIM experiment [17] was in particular sensitive to intermediate mass magnetic Monopoles with mass range of $10^5 < M < 10^{12}$ GeV. This sensitivity is because it was on a mountain top where there was little atmosphere to absorb low mass monopoles. In Fig. 1.1 the phase space of their sensitivity appears and they had 4 years of exposure and calculated 90% CL on the upper limit of 1.3×10^{-15} $cm^{-2}s^{-1}sr^{-1}$.

NOνA provides a unique opportunity to because of the large surface area of the detector and because the far detector is on the surface so it allows for intermediate velocity monopole to be detected. more about this will be in chapter 2.

Chapter 2

The NOνA Experiment

NOνA is a long baseline neutrino oscillation experiment using the NuMI beam at Fermilab to measure the $\nu_\mu \rightarrow \nu_e$ transition and the antineutrino counter-reaction. The experiment is composed of two identical functionality detectors located 14.6 mrad off the central axis from the NuMI (Neutrinos at Fermilab's Main Injector) beam. The Near detector is 300 t and is located 1 km downstream from the beam source at Fermilab. The Far detector is 14 kt and is located 810 km away at Ash River, Minnesota. The main goal of the Far Detector is to allow measurements of neutrinos after oscillations. Figure 2.1 shows the geographical location of the NOνA detectors.

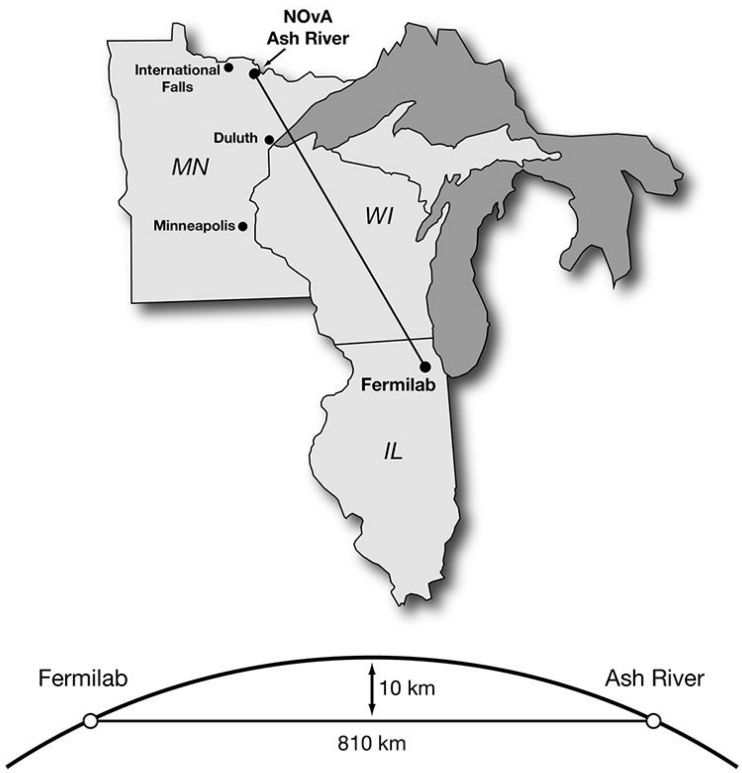

Figure 2.1: Geographical location of the NOvA detectors, this shows the location of both detectors, the Near Detector at Fermilab in Batavia, Illinois and the Far Detector in Ash River, Minnesota. [23].

2.1 Far Detector

The NOνA far detector consist of 896 planes of extruded highly reflective polyvinyl chloride cells. The planes alternately horizontal and vertical orientation to provide a three-dimensional structure. The detector consists of PVC plastic cells filled with liquid scintillating solution. The active material is about 65% of the detector mass. The two detectors are functionally identical in order to reduce systematic error in neutrino oscillation studies, see Fig. 2.4.

The PVC cell cross-section is rectangular with an area of $4\,\mathrm{cm} \times 6\,\mathrm{cm}$. The length of the cell spans the entire width or height of the detector, depending on the orientation of the plane. The goal is to increase spatial resolution so the hits can be localized to the cross-section size of one cell. And using materials that are constructed of low-Z material (PVC and oil) so that electromagnetic showers from ν_e appearance would extend across as many cells as possible, to allow the separation of ν_e-induced showers from NC-induced gammas. Each 16 PVC cells structure extruded together as in Fig. 2.2.

Figure 2.2: Schematics of PVC extrusion, extrusion is in the corner. Ends and middles are both just ends of single extrusions, so they have identical plastic and scintillator [18].

Every two extrusions are glued together to form a 32-cell wide module, as shown in Fig. 2.3. Modules are glued together to form a single plane. Then planes are oriented such that the beam is parallel to the plane normal vector.

The geometry of the detector allows the usage of Cartesian coordinates. The local detector coordinate system considers the NuMI beam as the Z-axis, height as Y-axis, and the remaining axis is the X-axis. As the beam points approximately toward the north, the X-axis happens to be in the direction of the west. This frame allows each plane to locate events in either XZ plane if plane cells are in vertical orientation or YZ if they are horizontal. The geometry parameters of the detector are summarized in Tab. 2.1.

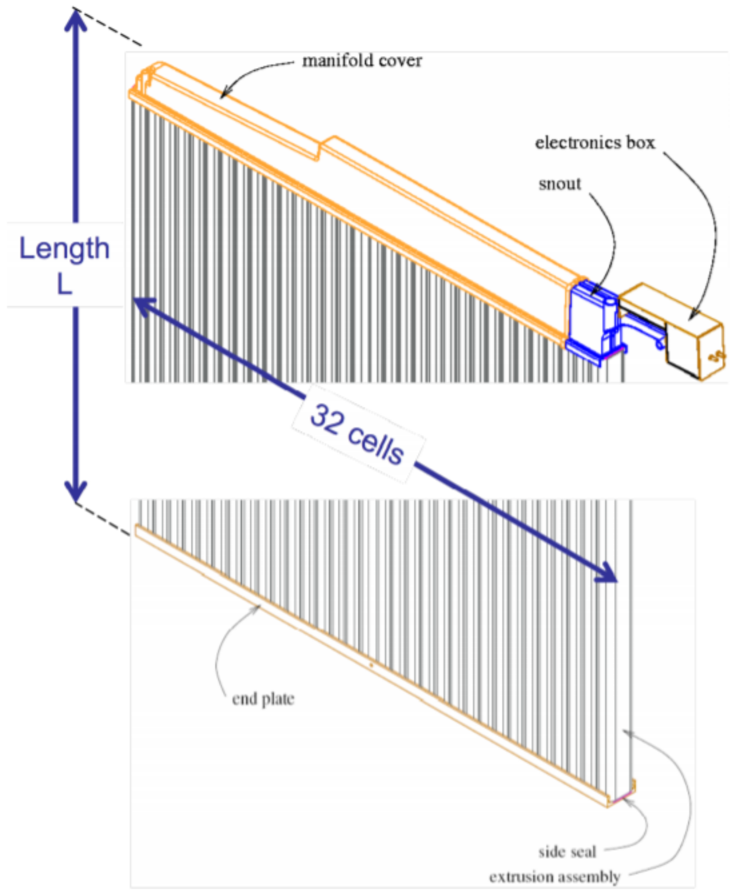

Figure 2.3: A side on view of an extrusion module constructed from two extrusions of 16 cells, an end plate, a side seal, a manifold cover, a snout and an electronics box [18].

NOνA's surface area is larger than other monopole search experiments, except IceCube. Table 2.2 compares the surface areas of different experiments. This is one of the advantages of NOνA for a magnetic monopole search as a larger surface area leads to larger acceptance.

Quantity	Value
Number of Planes	896
Cells per Plane	384
Cell Depth	5.64 cm
Cell Width	3.60 cm
788	6344
Size (Z)	[0, 5962] cm
Size (Y)	[-749, 765] cm
Size (X)	[-758, 765] cm

Table 2.1: Parameters of detector geometry summary [14].

Experiment	NOνA	MACRO	SLIM	OHYA
Surface Area (m^2)	4082	3482 [20]	427 [21]	2000 [22]

Table 2.2: The projected surface area of the NOνA far detector with other monopole experiments

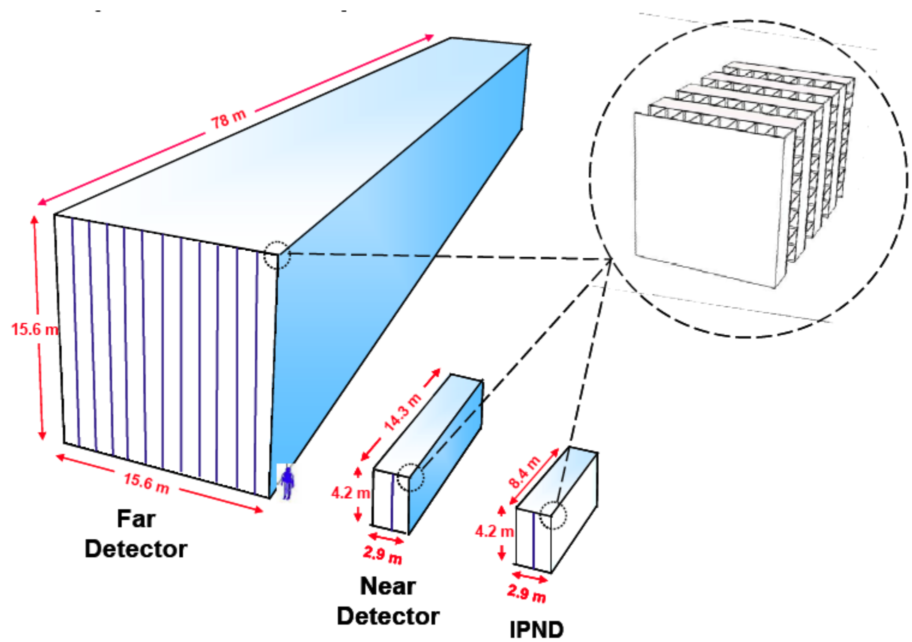

Figure 2.4: Comparison between Near and Far detectors size, The Far Detector is larger in size but they are functionally identical. The Near Detector is close to the beam source so it does not be to large like the Far Detector [14].

2.2 Near Detector

The Near Detector (ND) is located at Fermilab, Batavia. It is about 1 km from the beam target and composed of two different sections. The first section is a fully active region; each plane in the region consists of 3 modules with a total cross-section area of 3.8 m$\times$ 3.8 m. The total number of planes in this region is 192 and a length of 12.7 m. The ND has the same structure as the FD but with a smaller size, see Fig. 2.4. It is used for beam analyses [23].

The ND is an underground detector, unlike the FD, which means it is less affected by cosmic rays, which helps in reducing background noise. The close proximity of the ND to the beam provides the opportunity to acquire high statistics measurements of neutrino cross-sections. However, it is not useful for a magnetic monopole search because of its small size.

2.3 Data Acquisition System

NOνA uses a data acquisition system (DAQ) to get a continuous readout from the front end electronics and software triggering without dead time. The DAQ system records the following event types:

- Neutrino events from the beam: NOνA is a neutrino experiment with the main program focus on determining neutrino oscillation parameters such as the mass hierarchy.
- Calibration Data: It is required to get random samples of data for calibration purposes at $\sim$100 times the rate of beam spill data. Cosmic ray muons are recorded as part of this calibration process.
- Exotics physics: record signals like magnetic monopoles events which are the main analysis in this work.

The downstream buffer farm can store data for 20 seconds or more while giving triggers a chance to make the decision whether or not to save this data, based on the trigger design for physics of interest. For All the triggers (including the slow monopole trigger) is working with 5 ms blocks of data.

2.3.1 DAQ Data Formats

The raw data in the NOνA experiment has a hierarchical concatenation of data blocks that correspond to each level of the data acquisition system chain. The order is of the following according to our analysis:

- **Run**: The Run is a sequential collection of data of a certain period of time. The order is usually in terms of several hours. Each run contains information about the trigger and the detector (FD or ND). It has information to describe the trigger and time parameters of the DAQ system.

- **SubRun**: There is a size limit on the files written out by the data stream, and when reached, a new SubRun is started and the old one is stored in a raw data file. The current limit is either one GB or one hour time. If the data stream does not reach the size limit in this given time, a new SubRun will start. a collection of 64 SubRuns will form a given Run, and then a new Run will start automatically.

- **Event**: It is data object that records detector activity at a certain time. The time range depends on the trigger design and how it records the data. It contains information about triggering information (physics of interest), timing, and data block of the specific trigger. Events for this thesis purpose are either monopole events or minimum biased triggers that are events that are used to overlay simulated monopole events. These overlays are drawn from Supernova trigger events.

- **Trigger**: It contains information about the trigger type, the time when the trigger was issued, and other times that of interest regarding the trigger. It also contains information about the trigger source. This information is essential for the global triggering system for data retrieval and storage.

Chapter 3

The Slow Monopole Trigger

3.1 Data Driven Trigger System in NOνA

Every detector cell produces data that is buffered for real-time analysis by using the Data-Driven Trigger (DDT) system. The job of this system is to decide whether the data is of interest or to discard it. This decision is based on the event topologies. The DDT system is integrated into the DAQ system. Data is sent to Data Concentrator Modules (DCMs), and each DCM collects 5 ms of data from a local (2,098 cells) region of the detector. Then data is sent via a fast switch to the buffer node for temporary storage in RAM where it is combined with data for that same time period from all the other locations in the detector, forming a complete picture of detector activity for that 5 ms of time. A DDT process looks at that data to see if it wants to issue a trigger request for some part of data, and any trigger process might request that part of the time block to be sent off to form an event to be written by the data logger.

The DDT system in NOνA executes a full-featured reconstruction and analysis suite based on the ART framework [28]. The DDT works in parallel on each buffer node. There is a shared memory segment where it receives all the data from the buffer node, storing 5 ms sized chunks of complete detector data called "milliblocks" in a shared memory segment accessible by a number (currently 13) of different real-time analysis processes. The shared memory acts like a milliblocks queue for the DDT. This circular buffer depth is constrained by the available shared memory in the memory segment. However, due to computational limitations, the queue can be full, and in that case, the oldest milliblock is overwritten. This creates a problem that we might lose data before triggers make a decision. To process the data faster, we run eleven different instances of the DDT in parallel, each with its own CPU core. All of these trigger processes read the data from the same memory segment with each working on a different milliblock. Even so, it is sometimes not possible to reconstruct all the data, sometimes resulting in missed milliblocks. This causes missing data sometimes, so This analysis must account for it to calculate the overall efficiency

There are two monopole triggers; one is for very subluminal monopoles, and the other for faster-moving exotic but highly ionizing particles. The latter focuses on the fast, highly ionized monopoles. However, triggers with different algorithms issue different time windows when they operate on the same data milliblock, resulting in data sent to separate data-streams to be permanently stored. With 94 buffer nodes, the trigger decisions have to be made in about 6 seconds, or the data will be lost (discarded). Every trigger decision is independent of other decisions on the same block of data. It is common that a data block can have more than one trigger so that it will have multiple trigger messages for them. This practice will reduce the time as it is not necessary to wait until all triggers decisions are completed. Figure 3.1 shows an example of execution time for primary triggers over a period of 12 months.

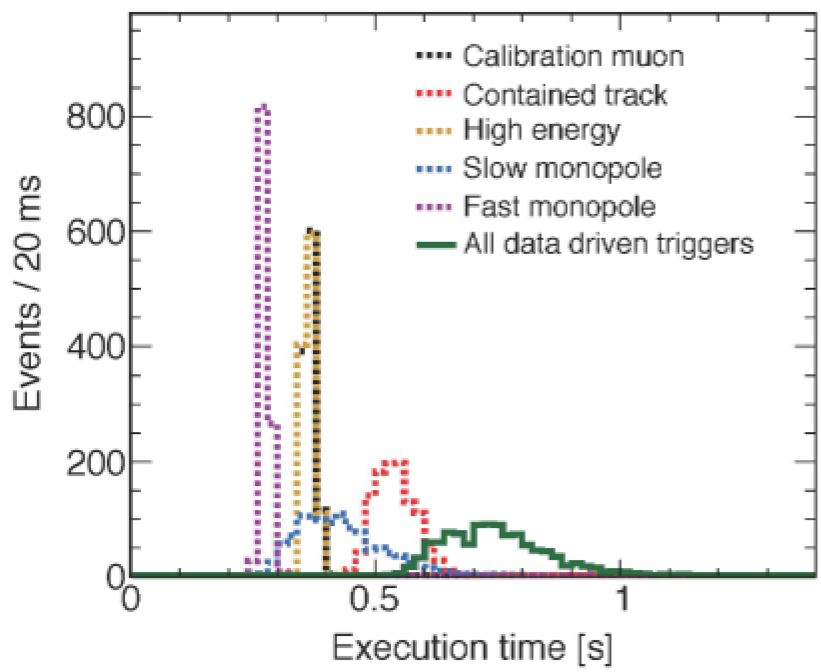

Figure 3.1: execution time for primary triggers (including slow monopole trigger) over a period of 12 months. It shows that the average time to decision is less than 1 s [26].

In Fig. 3.2, an example trigger algorithm is shown. This system takes 5 ms-long raw data from the shared memory and injects them in the ART framework. ART is used to run several software module in series: an unpacker translates the raw data format to one suitable for the physics algorithm, a filter module that uses a hough tracking algorithm to identify interesting events. A module then sends the decision messages to the global triggering system. Because of the ART framework compatibility, trigger algorithm code can be used in the offline mode for adjustments and tests before any upgrade. A filter module is used to partition detector hits into separate XZ and YZ views. For each view, the Hough parameters [37] for each pair of detector hits are calculated, and the peaks in Hough space resulting will be identified as track candidates. This algorithm is particularly useful in our analysis, as it has the ability to identify slow-particles tracks like slow monopoles in the far detector.

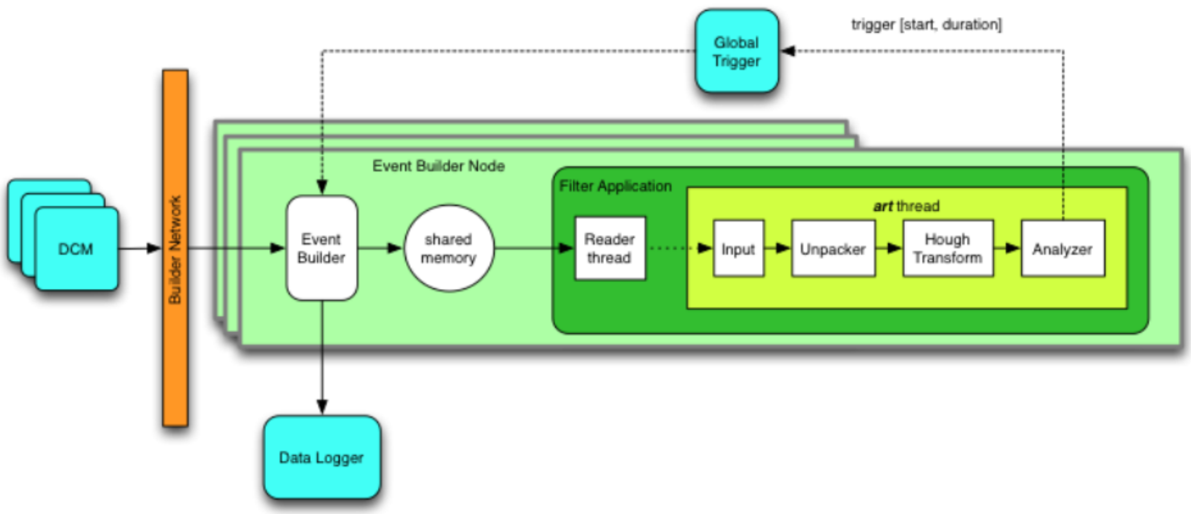

Figure 3.2: schematic view of NOνA Data Driven Trigger system. This example algorithm shows the flow of execution of system from receiving data from DCMs and performing filtering process, hough tracking and other physics algorithms using several analyzer modules [25].

The average time to decision quantity $< t_{dec} >$ is how long it took the trigger to look in that 5 ms block for its analysis. It is dependent on T_{DAQ} which is the period of data arriving at each buffer node, the number of buffer nodes N_{node} in the system and the number of filter analysis applications M_{filt}. the relation is estimated as follows:

$$< t_{dec} >= N_{node} M_{filt} T_{DAQ} \tag{3.1}$$

The number of allowed filter analysis applications to run is set to be 13, which is based on the CPU core optimization available at each buffer node. For the data acquisition period of this analysis, $M_{filt} = 13$ and $T_{DAQ} = 5$ ms and the number of buffer nodes was 94, which means that the average time available to reach a decision is about 6.1 seconds. The number of different triggers is tuned to account for this time constraint.

3.2 The Slow Monopole Trigger Algorithm

The slow monopole analysis is concerned with low-velocity monopoles, so the range of β (particle velocity over the speed of light) is small, typically between 10^{-2} to 10^{-4}. The slow monopole trigger was designed to take into consideration certain challenges: 1) adjacent hits have large time separation, and this requires a large time window to group all the hits that belong to the same monopole event. 2) The number of cosmic-ray background events is large. Figure 3.3 shows these challenges.

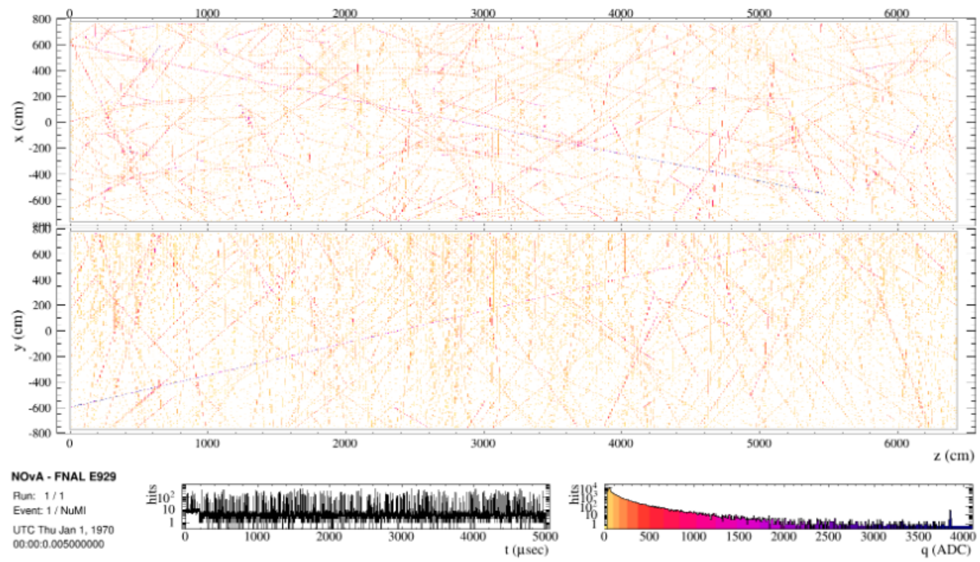

Figure 3.3: Simulation of magnetic monopole with mass= 10^{16} and $\beta = 10^{-3}$ in the NOνA far detector within a 5ms millislice, with overlaid cosmic rays and detector noise. The monopole track is easily separable from cosmic ray background due to timing and pulse height information. The top (bottom) part of the top figure shows the energy deposited in the vertical (horizontal) cells. The bottom two plots show the time of arrival with the millislice of the hit cells (left) and the energy spectrum of the hit cells (right) [27].

The large time window problem makes it impossible to reconstruct all the tracks within the entire millislice to find a slow monopole track. An algorithm is developed relying on the fact that cosmic rays are mostly fast muons traversing through the detector within one 50 µs time slice so it is better first to find the cosmic-ray muons slice-by-slice and eliminate all cell hits associated with the track. This leaves a slice free from cosmic rays and containing only noise, and any potential monopole candidate, if any. This is done by the offline reconstruction algorithm to save some trigger time.

The data analyzed by the DDT corresponds to a 5 ms readout window. The slow monopole trigger searches in live data and trying to identify the tracks that are consistent with slow monopole tracks. The trigger considers detector pairs of hits for each event. Due to the time limits discussed previously, the trigger has limited time to make a decision. The trigger looks for surface hits by finding hits on both XZ and YZ views. The hits in the two views must be adjacent in (z,t) for the other view. The trigger is currently looking for hits in XZ view that have adjacent hits in (z,t) in YZ view, then uses the hits in the XZ view to construct the track. The next step is to look for the hits between the original entry and exit hits in a 20 cells wide range. The trigger looks for gaps between hits in this range and identifies the maximum plane and cell gaps among them. The maximum plane gap is along the z-axis, and the maximum cell gap is along the x-axis. The trigger rejects any pairs with a plane gap of more than 30 planes or a cell gap of more than 20 cells because it is not consistent with slow particle track. The trigger iterates over all pairs of hits on the surface of the far detector. The trigger considers only every fourth pair when deployed because of computational limitation preventing the trigger from having time to look for all of the surface hit pairs. There is a requirement that the surface hits must have separation in space and time to originate from a track with β less than 5×10^{-3} because it focuses on slow tracks only. The method used here should be efficient, even thcough the trigger is looking for the tenth pair as the monopole track is expected to have many hits on the surface [34].

The period of time that is the subject of this analysis is the first 8 months in which the electronics were run at a higher gain than when originally deployed. Due to computational limitations, the trigger is checking over only every fourth track candidate. For this period, the minimum ADC value (a digitization value proportional to the light deposited in one cell) for a hit to be considered increased from 150 to 225.

Chapter 4

Search For Magnetic Monopoles Analysis

4.1 Introduction

The search for slow magnetic monopoles occurs in the NOνA far detector. The search algorithm is devised for slowly moving particles in general, not just the slowly moving monopoles. The current work is to investigate the difference and the potential improvement of the search with the new high gain data taken compared to the original low gain analysis [34]. There are a number of current limitations with the original analysis which could be loosened to increase the analysis' efficiency within data and Reconstruction Algorithm. The most important is the ADC cut and that the trigger takes only every fourth track. An analysis of how the total efficiency could be improved and the potential improvement of the new data is studied, and the results are presented in this chapter. Also, reconstruction and data analysis procedures are explained.

4.2 Magnetic Monopoles Simulation

The NOνA software is implemented under the ART Framework [28], which is a suite of libraries, tools, and applications for processing detector's events. The ART framework is developed and maintained by the Fermilab computing division. The simulation generator the software used is "Geant4" [29]. It simulates the propagation of particles throughout the detector with custom NOνA software for detector geometry and detector response simulations. The energy deposited by simulated monopoles is converted to scintillation light using calculations as described below. The response of the detector electronics to that light is then simulated, and converted to a digital ADC count that is proportional to the energy deposited in each cell. Scintillator light is thus converted into time/charge pairs stored for later use. The output is similar to raw data, and we can use the event display module to show both MC simulated data and real data. In Fig. 4.1, an example of an event display is shown. The event display gives a graphical representation of events inside the detector and is used to visualize simulated as well as real data.

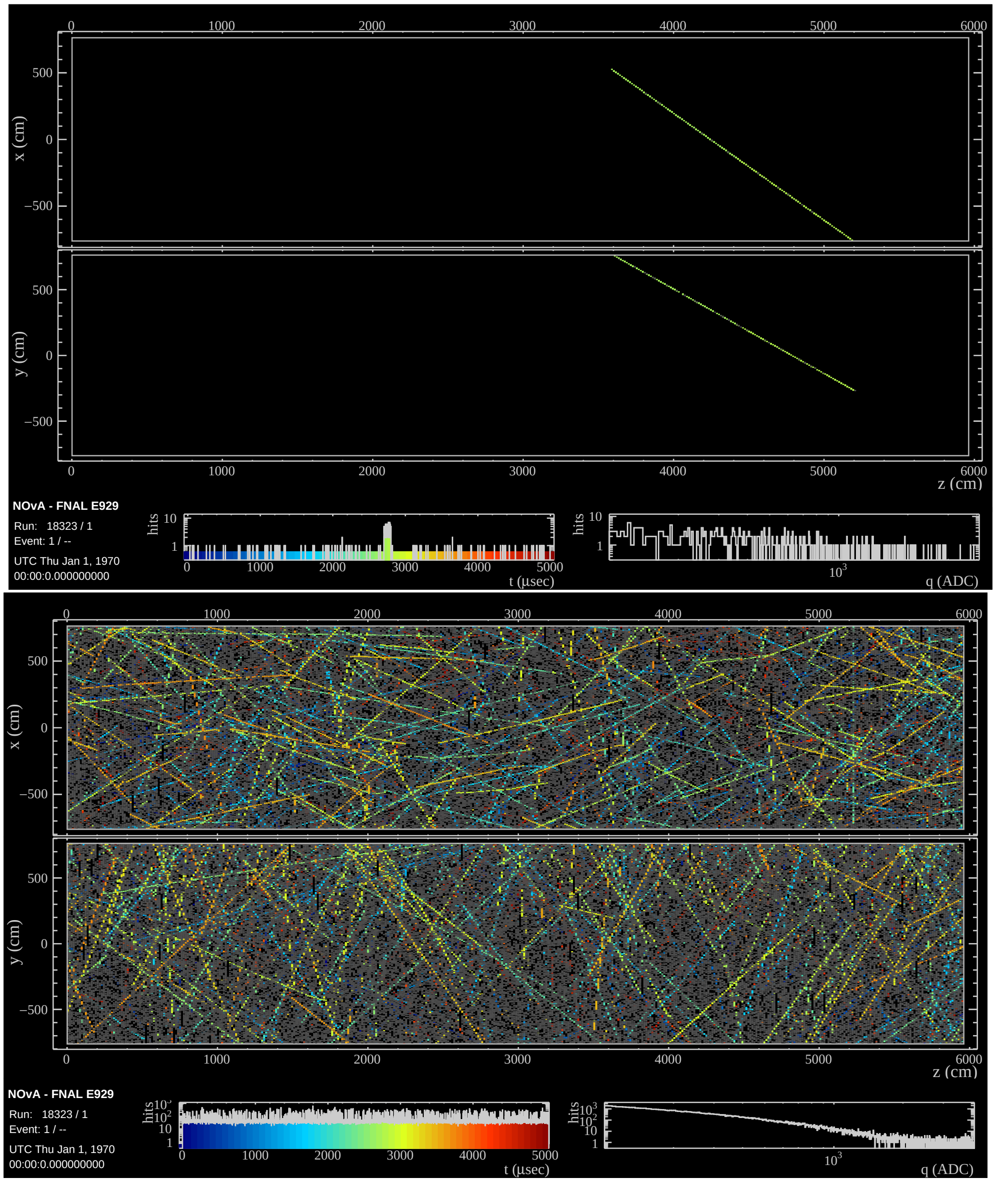

Figure 4.1: The event display shows the energy and time response of all the channels in both horizontal (y) and vertical (x) planes. Each hit is colored based on its value in units of ADC counts, representing the uncalibrated energy deposit. The top is an event display of a simulated non-relativistic ($\beta \sim 10^{-3}$) monopole's trajectory in both XZ and YZ views. The bottom is the same simulated monopole event overlaid with 5 ms of minimum biased data from supernova trigger events.

The package used for the simulation of magnetic monopole propagation through matter is *G4mplIonisationWithDeltaModel* package written by A.V. Bagulya et al [30]. There is no magnetic field in NOνA, and the earth magnetic field is negligible. The important energy loss processes in magnetic monopoles are the ionization and atomic excitation processes. There is a modification to the original package to correct energy loss by slow monopoles by using the following approximation:

$$\frac{dE}{dx} = 45\rho n_g \beta (GeV/cm) \tag{4.1}$$

Where ρ is the density of monopoles in units of g/cm^3, and n_g is the number of Dirac magnetic charges. This approximation works when the material is silicon only, so it is modified to the following equation inspired by the work of Ahlen and Kinoshita [31]

$$\frac{dE}{dx} = \frac{2\pi N_e n_g^2 n_e^2 \beta}{m_e c v_F}\left[ln\left(\frac{2m_e v_F \Lambda}{\hbar}\right) - \frac{1}{2}\right] \tag{4.2}$$

where $v_F = \frac{h}{m_e}(3\pi^2 N_e)^{\frac{1}{3}}$ is the fermi energy and Λ is the mean free path between the magnetic monopole and electrons for detectors and equals the Bohr radius r_0 for non-conductors [14]. The electron density of the scintillator used in NOνA is 2.96×10^{23} cm^{-3}.

The monopole's kinetic energy is very large relative to the energy lost in the detector, so we assume that the monopole will traverse the entire detector without stopping. The scintillation light does not scale linearly with energy deposited but is quenched for heavily ionizing particles. In the monopole simulation, the following empirical formula called Birks' law is used for accounting for this fact:

$$\frac{E_{visible}}{E_{true}} = \frac{\frac{dE}{dx}}{1 + \rho k_B \frac{dE}{dx}} \tag{4.3}$$

where ρ is the scintillator density, E_{true} is the energy deposited of charged particle, and $E_{visible}$ is the energy deposited that is proportional to the scintillation light yield. In this analysis, $k_B = 9.4 \times 10^{-3}\,\mathrm{g} \cdot \mathrm{MeV}^{-1} \cdot \mathrm{cm}^{-2}$ based on the work in [32].

The monopole is assumed to travel in a straight line; this helps to determine the track of the simulated monopole. The simulation steps the monopole through the detector inside the detector, and we can calculate the energy deposited in each cell using the standard way based on the path length through each cell. The simulation process stops at the moment of monopole exiting the detector. There are uncertainties on the measurements of slow monopole signals, as shown in [34], and to form a conservative flux limit we compensate for them by reducing the overall response by 10%. We do this by lowering the energy deposition according to the following equation

$$\frac{dE}{dx}_{sim} = 0.9 \frac{dE}{dx}_{theory} \tag{4.4}$$

The background of the current monopole search consists of cosmic rays that strike the detector at a high rate. Muons are the majority of the particles and penetrate more through the detector. NOνA usually uses the package CRY [33] for cosmic ray simulation. The package provides a flux of different particles (muons, neutrons, protons, electrons, pions, and photons). The particles list is passed to Geant4, which propagates particles through the overburden and the Detector. For this analysis however, we are not using CRY. We overlay with real minimum biased data as it is better in getting all the noise and cosmic rays showers than the CRY package.

4.2.1 The Monte Carlo Signal Data Set

The mass of the magnetic monopole is believed to be very high, so we set it to a very high value, and this would make velocity changes negligible along its path inside the detector. For the purpose of this thesis analysis, we have simulated 12,000 isotropic monopoles with a fixed mass of $M = 10^{16}\,\mathrm{GeV/c^2}$ and uniformly random variation of $9.99 \times 10^{15}\,\mathrm{GeV/c}$ in momentum. This gives us a uniform distribution of monopole speed within the range $\beta \sim (10^{-4}, 10^{-2})$. This simulated data is used to calculate and evaluate the trigger and monopole identification efficiencies, which will be discussed in section 4.4.2.

4.2.2 Monopole and Minimum Biased Sample

The simulation sample used in this analysis is a mixture of minimum bias data and simulated monopoles. We simulate monopole at various velocities in the slow range and then propagate them through the detector. We have one monopole per each event simulated in our sample. The next step is to combine this event with a 5 ms long non-bias data produced by the daily supernova test trigger. This approach gives us a sample of data consisting of overlaid events that contain the true monopole and a detector activity over a 5 ms period [35]. The MC sample can be used to evaluate the search algorithm and how well it can identify slow monopoles and construct their tracks, differentiating them from other background cosmic rays present in our sample.

4.3 Offline Reconstruction of Slow Monopole Tracks

In this section, an overview of the existing reconstruction algorithm of the slow monopole is given. In this work, the modification for this analysis are described later. The overall schema of the process is that the algorithm removes all cosmic rays moving with a speed of light and forms a single monopole cluster. The monopole cluster is divided into several monopole slices. Then we look for a track that looks like a monopole in these slices to form a monopole track.

4.3.1 Monopole Cluster

We start the process by collecting the data from the slow monopole trigger or by using the MC sample prepared as in the previous section. The first step is to remove cosmic rays moving at the speed of light, which are most of the hits. We are using the "Window Tracker" algorithm developed by the NOνA collaboration [36], and it identifies most of the cosmic rays tracks, and then we remove all the hits associated with these tracks.

The second step is trying to reduce the hit multiplicity by removing all the hits with a specific ADC count. The standard value is 100 ADC, and the trigger algorithm removes all hits with ADC count less than 150, so we choose a smaller value for the analysis. The majority of efficiency loss of the analysis is due to this cut, so this study tries to optimize the cut. One concern is that eliminating this hit removal cut results in a very long reconstruction time, so we should have a good balance between not removing too much of a potential monopole track and reconstruction time. More about the choices of hit removal values are in section 4.4.2.

The third step is to remove all of the isolated hits. We consider a hit isolated if there is no other hit within two cells and two planes. For this, we use cell and plane location in each detector view separately. We also remove any two hits that occur at the same location but at different times. After all three steps above, the remaining hits form a monopole cluster with one monopole cluster per event.

4.3.2 Monopole Slice

We need to find if any of the hits are correlated in space and time. A “window slicer” module was developed based on a time windowing algorithm with some modification of parameters. To be able to retain slow-moving particles, we allowed time windows to be 10 µs. In general, we require the minimum hits required for the slice is set to be ten and allowed plane-gap of ten planes. The hits collection produced by this window slicer module is called a “monopole slice”. There can be any number of monopole slices per event.

4.3.3 Monopole Track

When reconstructing large air shower events, it is found that it takes hours and makes it prohibitive to process with the search algorithm. A high energy sum requirement is placed on all of the monopole slices to remove these troublesome showers. We sum all the ADC counts in each slice and only retain slices with less than 1×10^6 ADC in the standard analysis on the low gain data. In this thesis for the high gain data, this requirement is increased to be 2×10^6 ADC.

Monopoles are assumed to be moving in a straight line as a heavy ionized particle. This tells us that we would like to identify straight-line tracks. A tracker module built on the Hough transform algorithm [37] is built for NOνA and is used for our identification. We use a minimum hit requirement of ten as a requirement for constructing a linear track.

The Hough module produces a list of peak locations in slope/intercept space with all the hits associated with each peak. Then, peaks that have a value larger than 40 are selected to form 2D tracks. To form these 2D tracks, we use the slope and intercept calculated from the peaks. Each detector view will have a 2D track, and we construct a 3D track by combining the two views. This is done as follows: First, a matching score is calculated from all the possible combinations of the two detector views that are based on overlap in the z-direction. Each hit in XZ-view that has a partner hit in the YZ-view receives a point. The partner is defined to be one plane away in either direction on the z-axis. The sum of all these hits is combined to calculate the final matching score. Currently, only the matches with a score of 20 or more are considered. The last step is to choose the match with the highest score to be the 3D track; then, the remaining matches proceed in order of their score. There is a requirement for the final track to contain a minimum of 100 hits to be considered a monopole track. The final match that fulfills this requirement is defined as a monopole track.

We want to determine the velocity of the track as we are looking for a slow-moving particle. At this stage, we have a 3D monopole track that is a collection of hits with a slope and intercept calculated from the Hough transform. Standard line fits are used to get the track velocity. These fits are applied to hits in each view separately to get the four velocity components defined as following:

- $\frac{dx}{dt}$: extracted from fitting (x,t) hits pairs from XZ-view
- $\frac{dz}{dt}|_{xz}$: extracted from fitting (z,t) hits pairs from XZ-view
- $\frac{dy}{dt}$: extracted from fitting (x,t) hits pairs from YZ-view
- $\frac{dz}{dt}|_{yz}$: extracted from fitting (z,t) hits pairs from YZ-view

Using the extracted four components we can calculate the track velocity using the pythagorean theorem:

$$v_{track} = \sqrt{\left(\frac{dx}{dt}\right)^2 + \left(\frac{dy}{dt}\right)^2 + \left(\left.\frac{dz}{dt}\right|_{xz}\right)^2} \tag{4.5}$$

where time is measured in nanoseconds, and distance is in cm. The tracks are sorted from the slowest to the fastest with the ability to have more than track per event-selection, although it is not likely to have two or more real monopole tracks in one event.

4.3.4 Event Selection

To determine if a particular event is of interest, it should pass through the following selection requirements in the MC truth information::

- number of simulated monopole hits in the XZ-view ≥ 20
- number of simulated monopole hits in the YZ-view ≥ 20
- z-extent of simulated monopole hits in the XZ-view ≥ 10 planes
- z-extent of simulated monopole hits in the YZ-view ≥ 10 planes
- track length of the simulated monopole track $\geq 10\,\text{m}$

where the length is defined as the distance between the first and last simulated monopole, hit when sorted by cell entry time.

The following are the selection requirements for the successful reconstruction of the simulated monopole:

- number of hits associated with the reconstructed monopole track in the XZ-view ≥ 20

- number of hits associated with the reconstructed monopole track in the YZ-view ≥ 20
- z-extent of hits associated with the reconstructed monopole track along z-direction in the XZ-view $\geq$ 10 planes
- z-extent of hits associated with the reconstructed monopole track along z-direction in the YZ-view $\geq$ 10 planes
- reconstructed track of the monopole track $\geq 10\,\mathrm{m}$

where the reconstructed track length is the diagonal of the smallest rectangular box containing all of the hits. The sides of this box correspond to the extent along the three detector dimensions of the hits associated with the reconstructed monopole track [34]. The reconstructed information's slowest three tracks are recorded, and the slowest track to pass the selection requirements is considered to be the primary monopole track in the particular event.

As discussed before, the monopole track is assumed to be linear, and the selection requirement for this is determined by fitting a line to the hits collection using linear regression methods. The squared correlation coefficient (r^2) is calculated for hits in each detector view separately. An r^2 value of one means that the hits lie perfectly on a straight line, and a value of zero means that hits are uncorrelated. We require a track to be considered a linear monopole track if it has $r^2_{min} \geq 0.95$. Another requirement for the analysis is that tracks should have a limit on the largest time gap possible. The purpose is to avoid having two separate unrelated tracks falsely clustered into one: a large apparent gap is a signature of a false track identification. We do this by sorting all hits within each track by time, and then we look in each view separately for the largest gap in time between hits (Δt_{max}) and Δt_{track} is the time difference between first and last hit. The time gap fraction will be defined as the following:

$$f = \frac{\Delta t_{max}}{\Delta t_{track}} \tag{4.6}$$

a perfect track will have an f value of zero, which means that there are no gaps in time along the track, and a value of one means that the two clusters of hits are independent. We require $f_{max} \leq 0.2$ for the track to be considered a linear monopole track.

4.4 Analysis

In this section, we will describe the work done on different data and MC samples to study the proposed improvements in the reconstruction efficiency of our search algorithm. In the next section, 4.4.2, the results for this analysis are presented. For the purpose of this study, we took the first eight months of the high gain data acquired by NOνA from October 2015 until June 2016. This corresponds to a live time of 231 days. NOνA has a policy to tune analyses based on MC and a small fraction of real data, so that we can limit human biases when searching for rare events. To get distributed sample that are easy to deal with, we chose to get every 29th subrun (Note that a full FD run consists of 64 subrun (0–63) of each run, which gives a uniformly distributed representative sample of our data. This subset will give us access to the full time span of the run range. The actual live time of this sub-sample is 3.7 days. This data is accompanied with MC data generated for the purpose of this study, as explained in section 4.2.1.

The purpose of the study is to understand parameter optimizations for better reconstruction efficiency. This is established using a comparison between the original reconstruction (described above) without parameter optimization applied to high gain data with a proposed new reconstruction with parameter optimizations applied to the same data. The schematics of the analysis are as following:

- running the original reconstruction algorithm on monopole data to create monopole reduced dataset
- running the original reconstruction algorithm on MC data to create MC monopole reduced dataset
- running the proposed reconstruction algorithm on monopole data to create a second monopole reduced dataset

- running the proposed reconstruction algorithm on MC data to create a second MC monopole reduced dataset

The proposed reconstruction parameter optimization is found to rely primarily on the adjustment of two parameters. We modified the hit removal ADC count parameter from 100 to 10. The main concern about hit removal adjustment is always the reconstruction time, which takes about double of time it takes per event if removed for the low gain study [34]. For our high gain data, removing this cut gives a very long time to construct event which needs further study in detail. The other parameter is we increased the ADC count sum removal discussed in section 4.3.3 from 1×10^6 ADC to 2×10^6 ADC. From trying different combinations of parameter adjustment, this one is the most significant in terms of improvement in algorithm efficiency. In Tab. 4.1, a summary of the main reconstruction parameters is given.

The key difference in choosing a smaller value for hit multiplicity removal is the reconstruction time; we tried optimizing this parameter, taking into consideration that very large reconstruction value makes running the analysis prohibitive. Table 4.2 gives an estimation of reconstruction time required per each event for different hit removal values.

Parameter value	Original	Proposed
Hit removal (ADC)	140	10
Isolated hits (cells/planes)	2	2
Time window (μs)	10	10
Window slicer (planes)	10	10
High energy filter (ADC)	1×10^6	2×10^6

Table 4.1: a comparison between the main reconstruction parameters for proposed and Original reconstruction models

Hit removal (ADC count)	Time (seconds per event)
100	~ 20
80	~ 23
50	~ 27
25	~ 32
10	~ 42

Table 4.2: Reconstruction time for different hit removal minimum ADC counts. It was made by making everything else constant. The times for different hit removal minimum ADC count is an average because of the variation depends on available NOνA computational nodes.

4.4.1 Monopole Flux Limit

In this work, we established a flux limit calculation for our subset of data to evaluate our reconstruction proposed model. The limit on the monopole flux is calculated according to possion distribution:

$$p\left(x\right) = \frac{e^{-\mu}\mu^{x}}{n!} \tag{4.7}$$

then integrating the equation with 90% confidence level

$$\int_{0}^{x} p(o/\mu)d\mu = 0.90 \tag{4.8}$$

where x is the 90% Confidence level limit, and p is the possion probability distribution function. For our analysis we use

$$x = \ln(10) = 2.3 \tag{4.9}$$

so that the 90% limit function will be this x over the analysis time-integrated acceptance

$$\Phi_{90\%} = \frac{2.3}{A} \tag{4.10}$$

where A is defined by this equation:

$$A = T \cdot \epsilon \cdot \Omega \cdot A_{projected} \tag{4.11}$$

and T is the integrated live time, ϵ is the overall efficiency, Ω is the solid angle coverage, and $A_{projected}$ is the projected surface area of the detector that is visible to the monopole [34].

The live time for the data is calculated from triggered raw data. In NOνA, data files have start and stop times so start and end times can be used for the calculation. Those times are stored in subrun header information and can be retrieved from raw files metadata. We require that the subrun must have non-zero events and start/end times to be non-zero to be counted in the live time calculation. We calculate the live time for our data and found it to be:

$$T_{live} = 320.451\,\mathrm{s} = 3.709\,\mathrm{days} \tag{4.12}$$

This value is what was used for the limit calculation in our result. Note that the full eight months of data will be used to calculate a much better limit once the analysis is approved to run over the whole dataset instead of this small sub-sample.

We have two coverage regions, which depend on the kinetic energy of the monopole calculated from the monopole's mass and velocity. If the magnetic monopole has enough energy, it can go through the entire earth without stopping. In such a case, it will have full coverage and could reach the detector from anywhere. Instead, if it has the energy to just make it through the atmosphere, then it will have a half coverage only being able to read the detector from above. Figure 4.2 shows the coverage solid angle function as a function of monopole parameter space (velocity and mass).

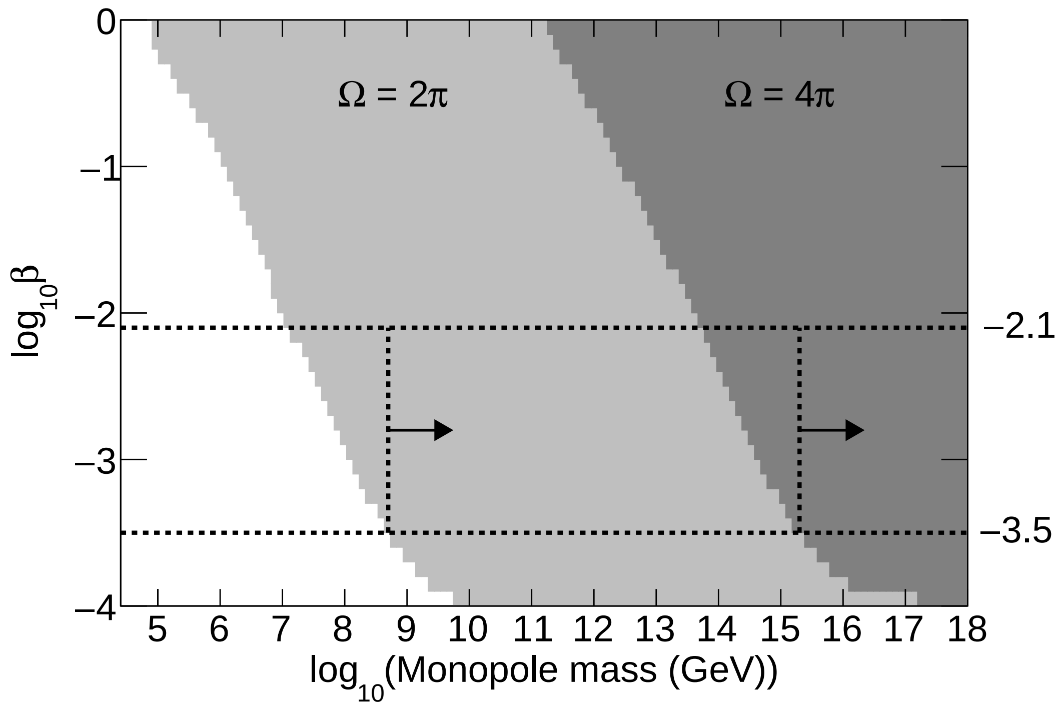

Figure 4.2: Coverage solid angle as function of monopole parameter space, $\Omega = 2\pi$ corresponds to the half coverage area while $\Omega = 4\pi$ corresponds the the full coverage. For half coverage this means that monopole enter the detector from above while full coverage means it can come from any direction [38]

4.4.2 Results

The results on the efficiency evaluation of MC reconstruction quality and overall reconstruction algorithm is presented here. We have a comparison between low (100 ADC) gain and our proposed optimization model. Figure 4.3 shows the distributions of the true information (black) generated from the MC sample for applying the reconstruction algorithm without optimization (original model).

As we can see from Fig. 4.3, the green shaded region indicates events that pass the signal selection and is plotted versus many important parameters. One particular feature is that our reconstruction works well within track lengths in the range (10 m-35 m). On the other hand, Figure 4.4 shows the same information for our proposed model.

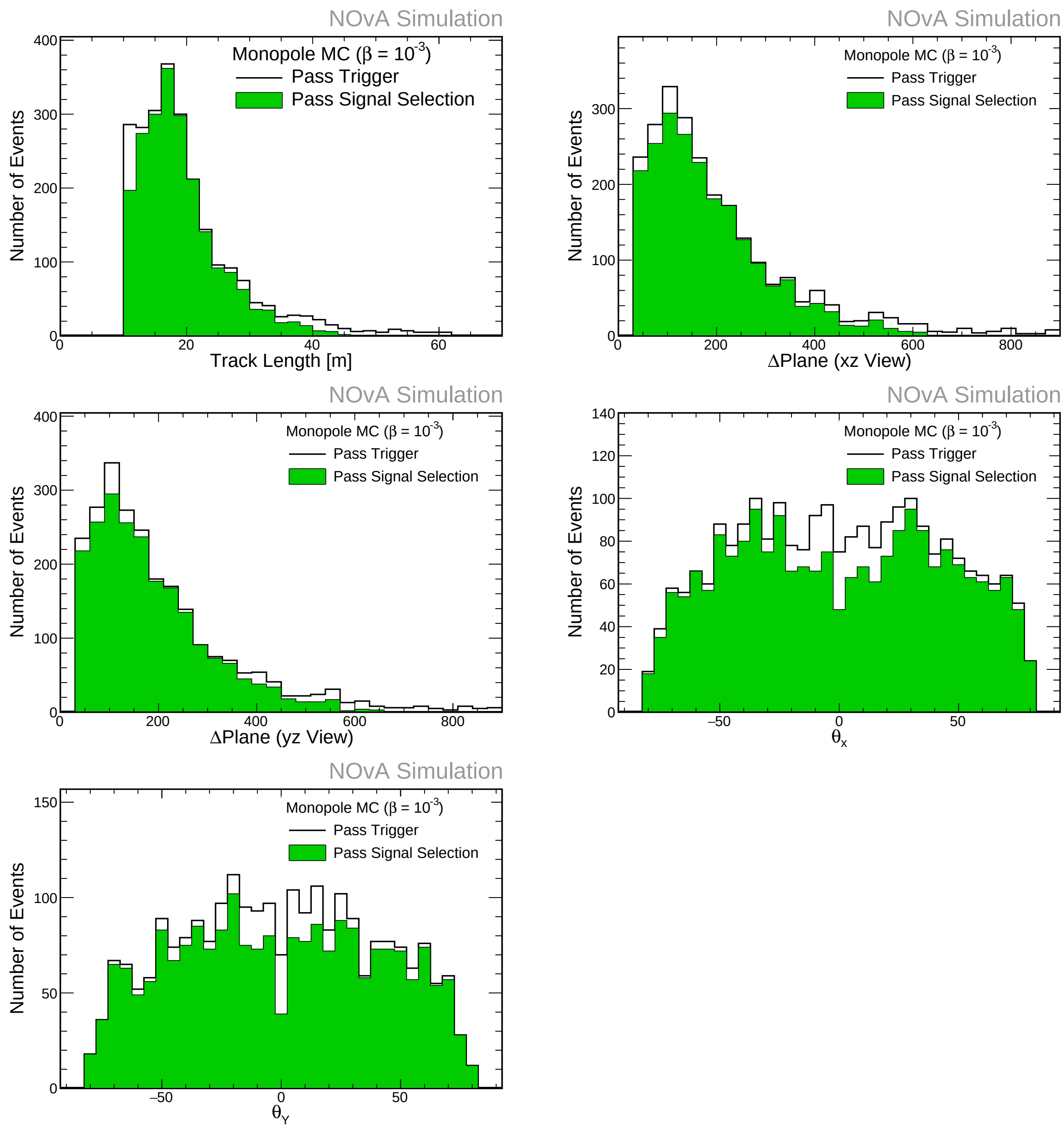

Figure 4.3: Histograms of the for original model gives the true information generated from all events that pass the trigger. The shaded green region indicates events that pass the signal selection which means it is well reconstructed events. y-axis is number of events and x variables are the selection variables explained in 4.3.4

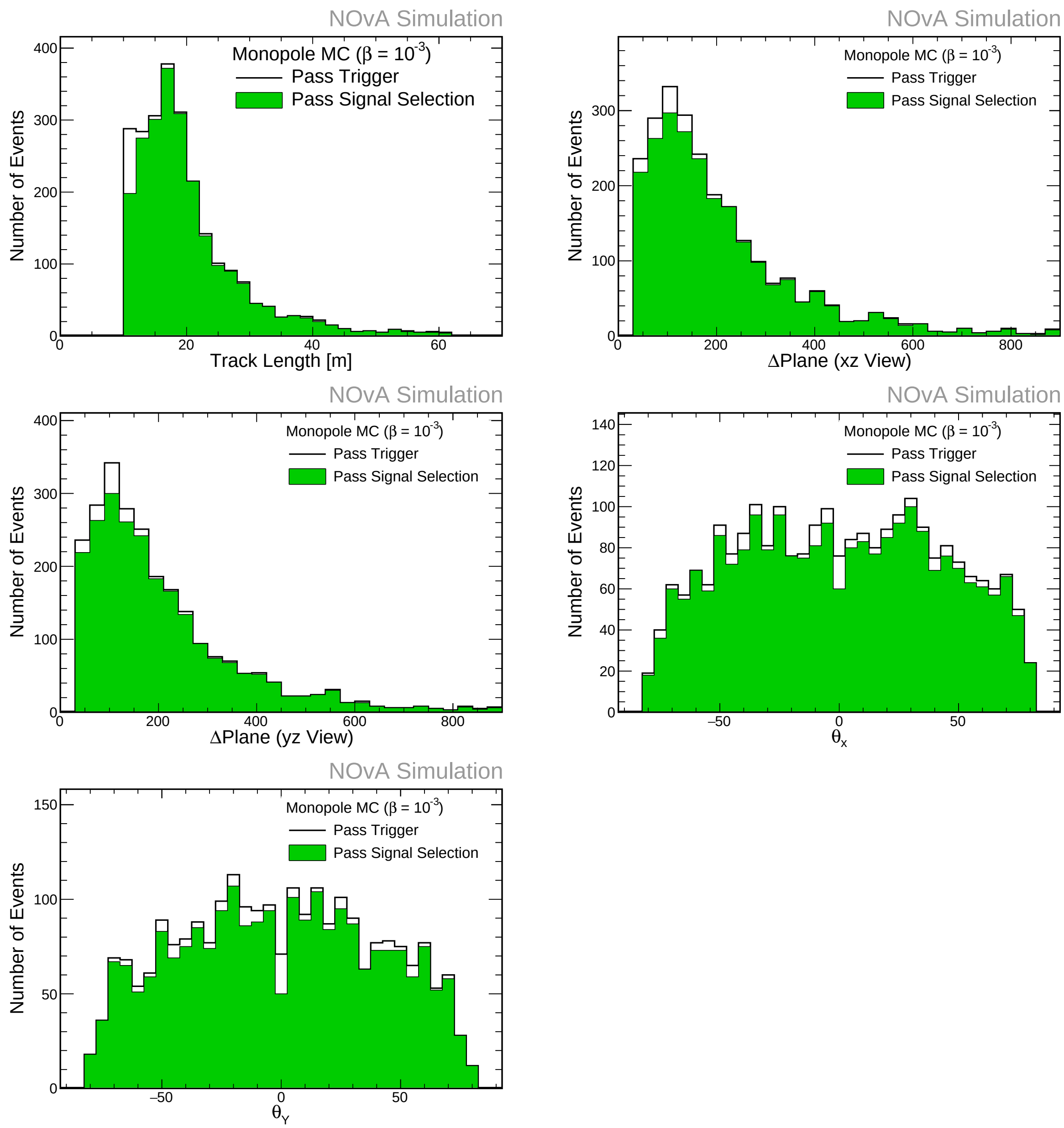

Figure 4.4: Histograms of the for proposed model gives the true information generated from all events that pass the trigger. The shaded green region indicates events that pass the signal selection which means it is well reconstructed events. y-axis is number of events and x variables are the selection variables explained in 4.3.4

As we can see, there is an improvement in the range of well-constructed track length for our proposed model seen by comparing the upper left histograms in Figs. 4.3 and 4.4. It is doing better per each view and per each angle. This qualitative behavior is supported by constructing an efficiency comparison graph for our β values. In Fig. 4.5, and efficiency for each β value and how well our algorithm works is presented for our two models.

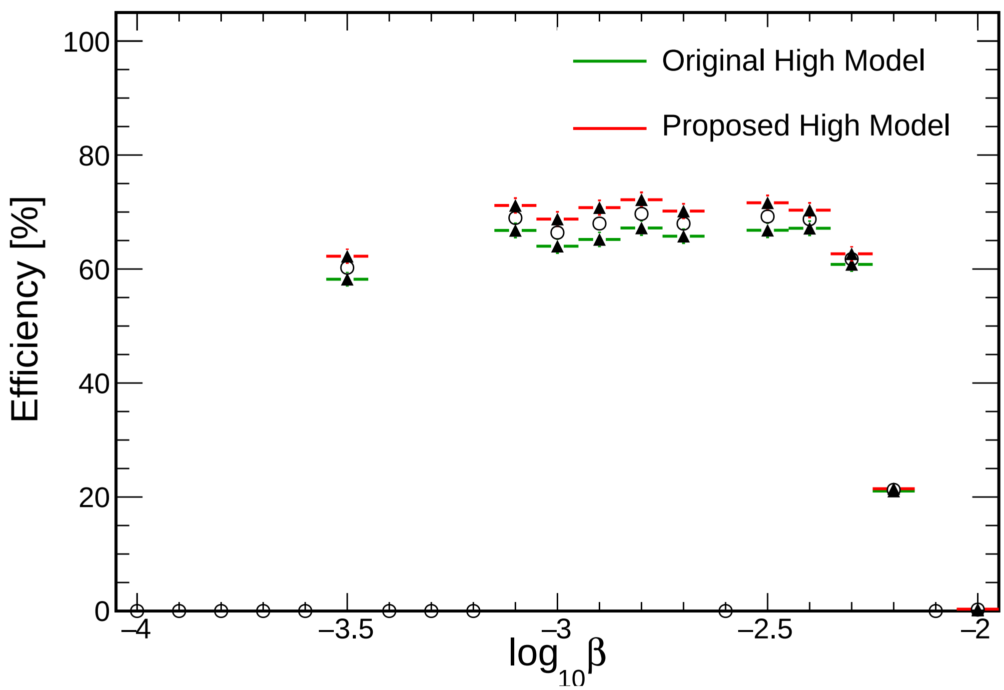

Figure 4.5: efficiency vs β comparison for our two models with error bars, for each velocity point we calculate efficiency of our algorithm to reconstruct tracks for the slow monopole velocity range. Circle dots are the mean value (average of the original vs proposed efficiency points).

The proposed model efficiency exceeds the original model at most points, which indicates better performance at these velocities. However, it does not add any significant improvement for the higher velocity monopoles. This is expected as this analysis is not designed to select those high speed monopoles as the slow monopole trigger discards fast track candidates. There is a current Fast monopole search optimized high speed monopoles [14]. In Tab. 4.3, the values for efficiency for each β is given, with the difference between our models gives definite improvements in numbers.

$\log \beta$	Proposed (%)	original (%)	Difference (%)
-3.5	62.25	58.20	4.05
-3.1	71.15	66.20	4.95
-3	68.76	64.00	4.76
-2.9	70.77	65.20	5.57
-2.8	72.16	67.20	4.96
-2.7	70.17	66.76	4.41
-2.5	71.62	66.80	4.82
-2.4	70.33	67.15	3.18
-2.3	62.67	60.81	1.86
-2.2	21.45	21.04	0.41
-2	0.32	0.16	0.16

Table 4.3: efficiency comparison table for our two models and the difference between them. This difference is the improvement we have in our analysis

The average improvement for our MC reconstruction quality is about 3.4 %. It is also important to note that this number does not have a deep meaning as monopole search is sensitive to β values, and not all monopole moving at different velocities will be reconstructed with the same accuracy. This comparison can also be extended to the low gain efficiency study in [34]. Figure 4.6 shows this comparison.

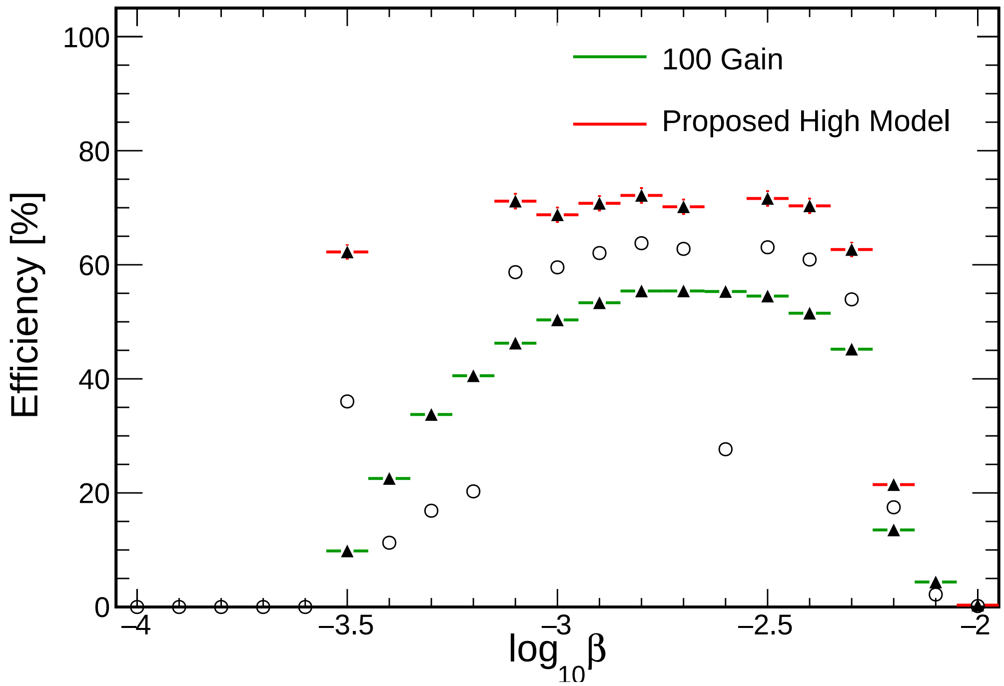

Figure 4.6: efficiency vs β comparison between 100 gain and our 140 gain proposed model with error bars, for each velocity point we calculate efficiency of our algorithm to reconstruct tracks for the slow monopole velocity range. Circle dots are the mean value (average of the original low gain vs proposed High gain efficiency points). efficiency goes to zero for high speeds as our algorithm is not sensitive to this region. Also, it goes to zero for $\sim \beta^{-4}$ as the trigger don' have enough hits because of the faint light signals.

The low gain analysis was conducted using more β points, but the trend for the two analyses are obvious. There is an increase in the efficiency of overall points. This qualitative behavior is also quantified in Tab. 4.4.

The Event selection requirements in 4.3.4 are the rules in which the Reconstruction

[1]negative value means that low gain efficiency is better and our model is worse for $\beta = 10^{-2}$

$\log \beta$	High gain (%)	Low gain (%)	Difference (%)
-3.5	62.25	9.83	52.42
-3.1	71.15	46.54	24.61
-3	68.76	56.33	12.43
-2.9	70.77	53.34	17.43
-2.8	72.16	55.40	16.76
-2.7	70.17	55.40	14.77
-2.5	71.62	54.51	17.11
-2.4	70.33	51.51	18.82
-2.3	62.67	45.20	17.47
-2.2	21.45	13.51	7.94
-2	0.32	4.38	-4.0[1]

Table 4.4: The table shows comparison between the low and the proposed high gain model.

algorithm are identifying tracks if they belong to a magnetic monopole or not. We need to see the event counts that pass various requirements for a selection of monopole. Table 4.5 shows the event counts for Event selection requirements placed on our MC sample using our proposed and original models. The "Total" row gives the total number of events in the sample. The "MC Hit Detector" row gives the number of MC events where the monopole deposits energy in at least one cell. The "MC Pre-selection" row are for the requirements described in 4.3.4. The "Data-Driven Trigger" row indicates all of the events that pass the slowmonopole trigger. The last three are for both data and MC and are described in the Event selection section as well. The "overall efficiency" is the fraction of slow events out of the total number of events.

$\beta = 1 \times 10^{-3}$		
Number of Events	Proposed	Original
Total	65,501	65,501
MC Hit Detector	62,985	62,985
MC Pre-selection	35,103	35,103
Data-Driven Trigger	28,847	28,992
Reco Pre-selection	22,167	20,692
Reco Linear	21,893	20,692
Reco slow	21,891	20,690
Overall Efficiency [%]	33.4	31.6

Table 4.5: The table shows the event counts that pass various requirements for the Event selection

4.4.3 Magnetic Monopole Flux Limit

Applying the proposed high gain model algorithm on the raw detector data in 4.4 for unblinded sub-sample of 3.7 days of exposure of high gain yields no magnetic monopole signals. None of the events fell into the signal region. Figure 4.7 shows the distribution of the full data sample together with the MC sample overlaid for comparison. It is clear that no data points are within the signal region indicated by the green line. No data points are within the remaining region after r^2_{min} cut of 0.95. Since there is no magnetic monopole, we proceed to set limits on the monopole flux. This exposure time is too low to be interesting but this work explains how it will be done once NOνA collaboration approves doing the analysis on all the data available.

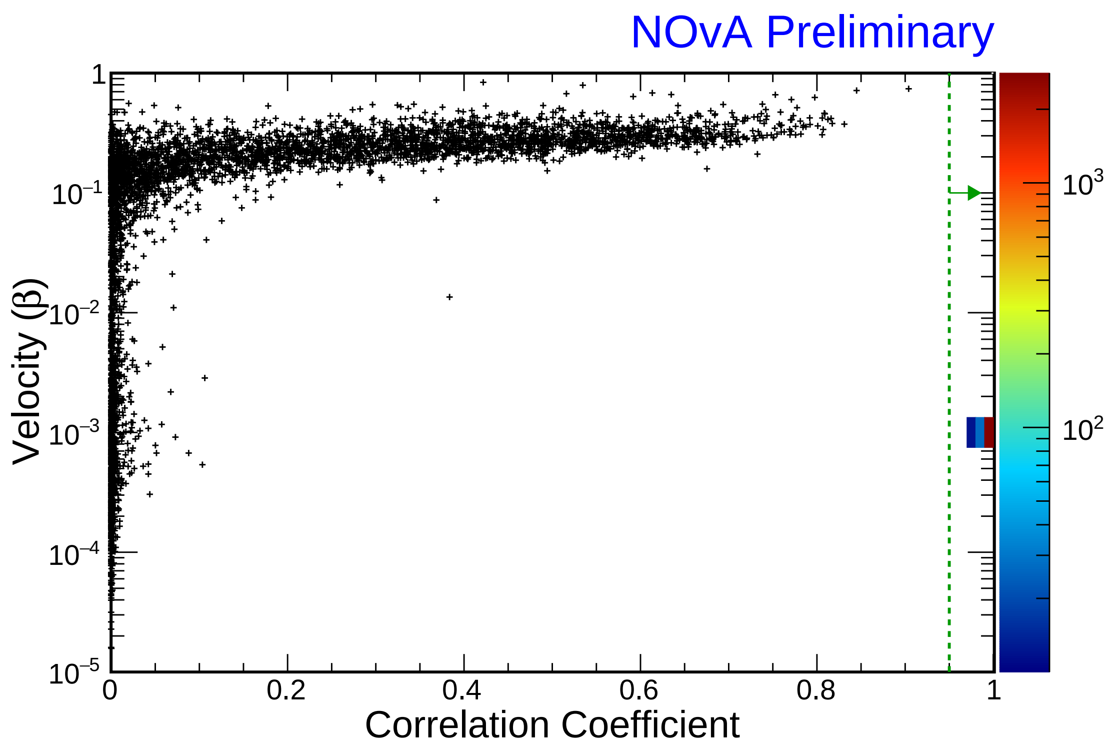

Figure 4.7: Scatter plot of β vs r^2_{min} for all linear event of data (black dots) and MC (heat map).This distribution shows no data events in the signal region indicated by the dashed green line.

To proceed with the limit calculation, we can calculate the limit for each individual velocity point using procedures described in Sec. 4.4.1. Figure 4.8 shows the limit on the magnetic flux that we yield for this analysis. The limit increases at high velocity is by design due to the trigger-level β cut of $5 \times 10^{-3} \sim 10^{-2.3}$.

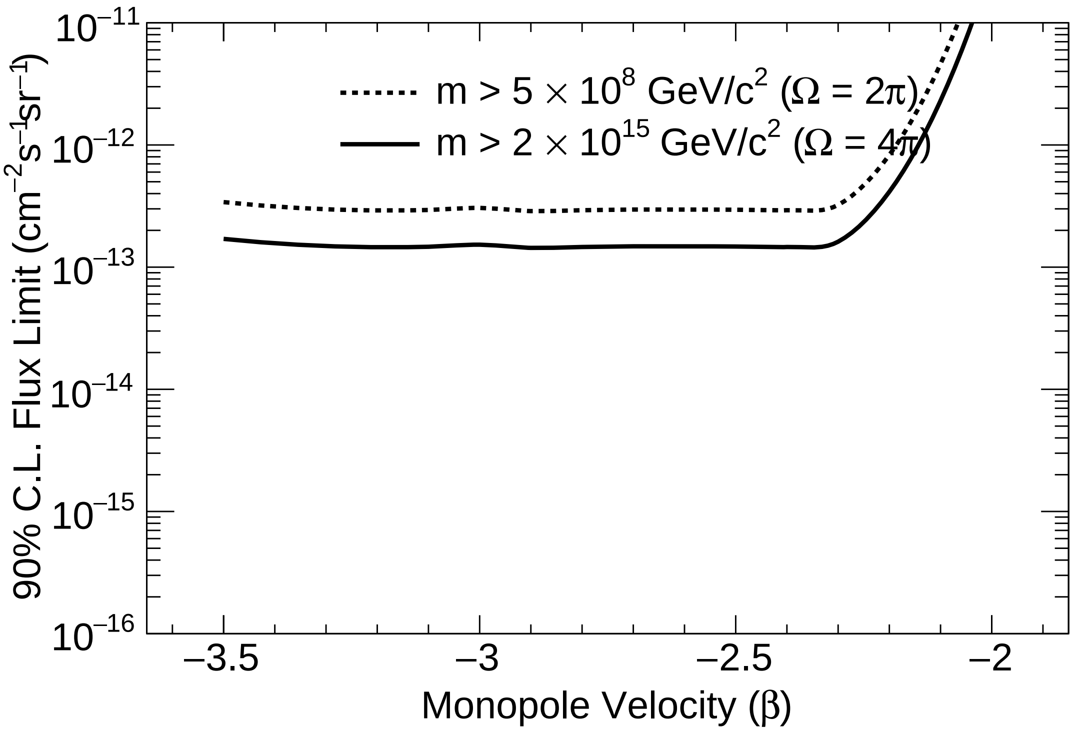

Figure 4.8: 90% C.L. upper limits on the magnetic monopole flux generated by applying our proposed model on our subset of the representative sample of high gain data acquired by NOνA Far Detector.

4.4.4 Conclusions and Future Work

This analysis gives results about the potential improvement of the slow monopole search reconstruction algorithm with NOνA Far Detector. This study was conducted on a small representative sample and presents improvement and should be applied to the full high gain data acquired. The estimation of live time of the full high gain dataset is about 1028 days, which will require more MC production and a lot of computational resources. The NOνA collaboration plans to carry on this analysis for the full dataset, and this will push the limit on monopole flux presented here. This analysis provides the groundwork for a a full analysis of high gain data. The work done here was on unblinded sub-sample representative for the full data and once the collaboration approves the analysis, it should be carried the same way to search for any monopole signal within this data or proceed with a more interesting monopole flux limit.

Bibliography

[1] Du Trémolet de Lacheisserie, Étienne; Damien Gignoux; Michel Schlenker (2005). Magnetism: Fundamentals. Springer. pp. 36. ISBN 978-0-387-22967-6..

[2] H. C. Oersted, "A Source Book in Physics" W. F. Magie, ed., Harvard University Press, Cambridge (1965) p. 437.

[3] A. M. Ampere, "A Source Book in Physics" W. F. Magie, ed., Harvard University Press, Cambridge (1965) p. 446.

[4] Maxwell, James Clerk. A Treatise on Electricity and Magnetism . Oxford, Clarendon press, 1873.

[5] P.A.M. Dirac, Proc. Roy. Soc. A 133, 60 (1931); Phys. Rev. 74, 817 (1948)

[6] R. Liu, A search for fast moving magnetic monopoles with the MACRO detector, Caltech Dissertation, 1995.

[7] Saha M N 1936 Ind. J. Phys. 10 141

[8] Wilson H A 1949 Phys. Rev. 75 309

[9] G. 't Hooft, Nucl. Phys. B 79, 276 (1974).

[10] A. M. Polyakov, JETP Lett. 20, 194 (1974).

[11] E. W. Kolb and M. S. Turner, The Early Universe, Addison-Wesley Publishing (1990).

[12] A. S. Goldhaber (Magnetic monopoles and cosmic inflation), (2005), arXiv:gr-qc/0512056

[13] Cabrera, Blas. 1982. First Results from a Superconductive Detector for Moving Magnetic Monopoles. Physical Review Letters 48(20): 137881.

[14] Wang, Zukai. Search for Magnetic Monopoles with the NOνA Far Detector. United States. doi:10.2172/1230047.

[15] M. Ambrosio, et al. (MACRO Collaboration), Eur. Phys. J., C25, 511 (2002).

[16] M. Aartsen *et al.* [IceCube], "Search for non-relativistic Magnetic Monopoles with IceCube," Eur. Phys. J. C **74** (2014) no.7, 2938

[17] Balestra, S., et al. "Magnetic Monopole Search at high altitude with the SLIM experiment," Eur. Phys. J. C **55**, 57-63 (2008)

[18] D. S. Ayers, et al. (NOvA Collaboration), The NOvA technical design report (2007).

[19] Adamson, P., et al. The NuMI Neutrino Beam. Nuclear Instruments and Methods in Physics Research Section A: Accelerators, Spectrometers, Detectors and Associated Equipment, vol. 806, Jan. 2016, pp. 279306, doi:10.1016/j.nima.2015.08.063.

[20] M. Ambrosio, et al. (MACRO Collaboration), Eur. Phys. J., C25, 511 (2002).

[21] S. Balestra et al., Eur. Phys. J. C55, 57 (2008).

[22] S. Orito, M Imori, K. Yamamoto, H. Yamakawa, T. Suzuki, K. Anraku, M. Nozaki, M. Sasaki, T. Yoshida, K. Kuwahara, et al., Phys. Rev. Lett., 66, 1951 (1991).

[23] G. K. Kafka, "A Search for Sterile Neutrinos at the NOνA Far Detector," doi:10.2172/1336405

[24] S. Kasahara, NOvA Data Acquisition System, in: Technology and Implementation in Particle Physics 2011 (these proceedings), 2011.

[25] Fischler, M. et al. 2012. NOvA Event Building, Buffering and Data-Driven Triggering From Within the DAQ System. Journal of Physics: Conference Series 396(1): 012020.

[26] Norman, A. et al. 2015. Performance of the NOνA Data Acquisition and Trigger Systems for the Full 14 KT Far Detector. Journal of Physics: Conference Series 664(8): 082041.

[27] Wang, Z. et al. 2014. Software Trigger Algorithms to Search for Magnetic Monopoles with the NOνA Far Detector. Journal of Physics: Conference Series 513(1): 012039.

[28] Biery, K. et al. 2013. Artdaq: An Event-Building, Filtering, and Processing Framework. IEEE Transactions on Nuclear Science 60(5): 376471.

[29] Agostinelli, S. et al. 2003. Geant4a Simulation Toolkit. Nuclear Instruments and Methods in Physics Research Section A: Accelerators, Spectrometers, Detectors and Associated Equipment 506(3): 250303.

[30] A. V. Bagulya, M. S. Vladimirov, V. N. Ivanchenko, and N. I. Starkov,Bulletinof the Lebedev Physics Institute, Vol.36, No. 5, 127 (2009).

[31] S. P. Ahlen and K. Kinoshita, Phys. Rev.D26, 2347 (1982).

[32] V. I. Tretyak ,EPJ Web of Conferences65, 02002 (2014).

[33] C. Hagmann, D. Lange, and D. Wright, In Nuclear Science Symposium Confer-ence Record, 2007. NSS07. IEEE Vol. 2, 1143 (2007).

[34] A.Antoshkin et al , NOνA Slow Monopole Analysis, NOvA internal note 22610, version 1, private access (2019).

[35] E. Song, Overlay Monopole MC and Real Cosmic Data, NOνA internal note 13831, version 1, private access (2015).

[36] B. Rebel, Window Tracking Algorithm for Cosmic Ray Muons, NOνA internal note 15977, version 1, private access (2016).

[37] Pozzobon, Nicola, Fabio Montecassiano, and Pierluigi Zotto. 2016. A Novel Approach to Hough Transform for Implementation in Fast Triggers. Nuclear Instruments and Methods in Physics Research Section A: Accelerators, Spectrometers, Detectors and Associated Equipment 834: 8197.

[38] "M.Frank et al , Slow Monopole Paper, NOvA internal note 43014, version 11, private access(2020)".